SATELLITE DERIVED INTEGRATED WATER VAPOR AND RAIN INTENSITY PATTERNS: INDICATORS OF RAPID CYCLOGENESIS

Lynn McMurdie and Kristina Katsaros

Department of Atmospheric Sciences
University of Washington, Seattle WA 98195

1. INTRODUCTION

Rapidly intensifying extratropical cyclones are accompanied by severe weather conditions and frequently develop over the data sparse ocean areas. Although operational numerical model performance has improved in recent years, the strength can be poorly predicted, due in part to an inadequate initial analysis (Sanders, 1987). Recent research has demonstrated the importance of moist processes and latent heat release in the development of these cyclones (e.g. Kuo et al., 1991). Hence, an adequate representation of the moisture fields appears to be important for accurate prediction of these storms (Reed et al., 1988).

Atmospheric water vapor and precipitation intensity can be retrieved over the ocean from satellite microwave radiometers. These fields have been used to delineate frontal zones (McMurdie and Katsaros, 1985; Katsaros et al., 1989), to characterize typical water vapor distributions and content in storms occurring in various oceanic basins (McMurdie and Katsaros, 1991), and to study moisture pattern evolution in the Gulf of Mexico following the passage of a cold front (Rabin et al., 1991).

In this paper, we examine integrated water vapor fields and rain intensity patterns derived from the Scanning Multichannel Microwave Radiometer (SMMR) and Special Sensor Microwave/Imager (SSM/I) for several rapidly deepening and non-rapidly deepening midlatitude cyclones in the North Atlantic. Our goal is to identify features in the satellite data unique to the rapidly deepening cases, and to explore how these data can potentially be used in the analysis and forecasting of these events.

2. DATA ANALYSIS

The SMMR and the SSM/I are passive microwave instruments on the Nimbus 7 and the Defense Meteorological Satellite Program (DMSP) polar orbiting satellites, respectively. Information on each instrument is presented in table 1. The algorithms used to calculate SMMR integrated water vapor (IWV) are given in Chang et al. (1984) and Petty and Katsaros (1990) for the SSM/I. They are valid over ocean areas and are as accurate as radiosondes within a rms error of 2.1 and 2.0 kg m^{-2}, respectively. Since accurate measures of rainrate are difficult to obtain from satellite, we use a normalized polarization difference (P_{37}) in the 37 GHz channel to indicate rain intensity for the SSM/I cases. It is defined as the measured 37 GHz vertically polarized brightness temperature (T_b) minus the 37 GHz horizontally polarized T_b divided by the clear sky T_b polarization difference. Low values (0.1 or 0.2) indicate high rain intensity and high values (greater than 0.8) indicate no rain. For the SMMR cases, a simple polarization difference in the 37 GHz channel is used to indicate rain.

Thirty-four North Atlantic storms that occurred during the winters of 1979 - 1981 (SMMR) and 1988 (SSM/I) are divided into two groups: 1) Rapidly deepening storms, where the storm experienced a deepening rate of 1.4 or greater for 24 hours (a deepening rate of one is defined in Sanders and Gyakum (1980) as a drop of 24 mb in 24 hours multiplied by (sin ϕ / sin 60°) where ϕ is the latitude of the storm); and 2) Standard storms, where the storm experienced a deepening rate less than 1.4. The NMC hemispheric surface analysis is used to determine the central pressure and the position of the surface fronts. Water vapor fields and rainfall intensity are compared during the incipient (more than twelve hours prior to the period of most rapid deepening) and deepening stages.

Table 1 - Comparison of SMMR and SSMI instruments

	SMMR	SSMI
Dates	1979 - 1985	1987 - present
Swath width	780 km	1394 km
Channels	6.6, 10.7, 18 GHz 21, 37 GHz	19, 22.2, 37, 85 GHz
Polarization	Vertical and Horizontal all channels	Vertical and Horizontal all channels, 22.2 in vertical only
Resolution (IWV, P_{37})	50 km x 50 km	50 km x 50 km

IWV and P_{37} fields from individual passes over a storm are analyzed as follows. Only the passes that sampled the majority of the storm near the low center are included in the study. Maximum water vapor content in the warm sector, or along the cold and warm fronts, is estimated from the IWV patterns by picking the highest contour (contour interval is every 2 kg m^{-2}) in the analyzed field along, or within 200 km of the frontal zones. In addition, the areal extent of the region of high water vapor content is estimated by counting the number of pixels greater than 30 kg m^{-2}, multiplying that number by the pixel resolution and rounding to the nearest 10^3 km^2. The region considered does not extend south of 25°N or 5° of latitude south of the southern portion of the cold front in order to include just the warm sector and frontal zones sampled by the satellite. The value 30 kg m^{-2} was choosen arbitrarily since it is approximately the average maximum IWV content for North Atlantic storms found by McMurdie and Katsaros (1991). For the rain intensity fields, the areal extent of the region of rain (quantified as P_{37} less than 0.8 for the SSM/I and 37 GHz polarization difference of less than 30°K for the SMMR cases) is calculated in the same manor. Maximum water vapor, areal extend of high vapor content and areal extent of precipitation from each pass over a storm are averaged together for rapidly deepening storms and standard storms. The averages in similar categories (e.g. maximum water vapor content during the incipient stage in rapid vs. standard cases) are tested to be significantly different using the two sample t-test.

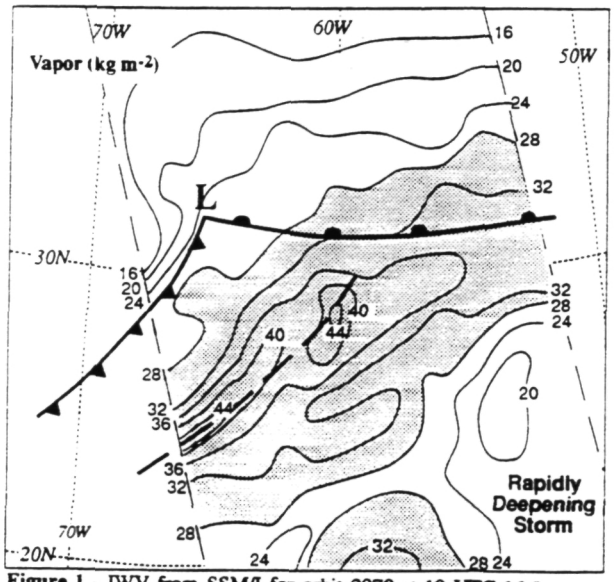

Figure 1 - IWV from SSM/I for orbit 2970 at 10 UTC 16 January 1988. The field is contoured every 4 kg m^{-2} and the region greater than 28 kg m^{-2} is shaded. Frontal analysis is estimated from the NMC hemispheric surface charts at 06 and 12 UTC 16 January.

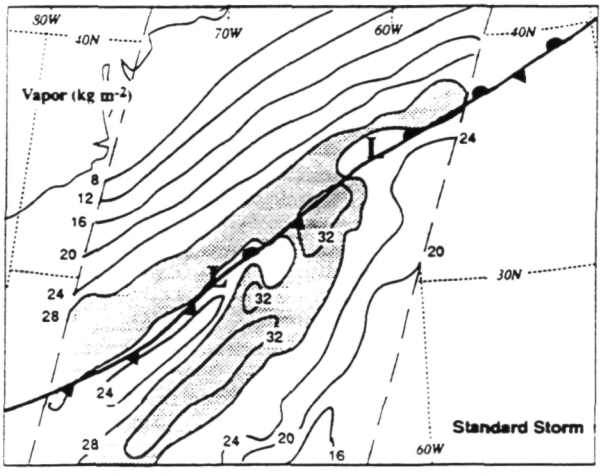

Figure 3 - IWV from SSM/I for orbit 3274 at 23 UTC 6 February 1988. The field is contoured every 4 kg m^{-2} and the region greater than 28 kg m^{-2} is shaded. Frontal analysis is estimated from the NMC hemispheric surface charts at 00 UTC 7 February.

3. WATER VAPOR

3.1 Rapidly Deepening Case: 15 - 17 January 1988

The surface low of this system developed from a weak trough of 1018 mb situated at 32°N 72°W at 00 UTC 16 January. At this time a strong shortwave trough was situated along the east coast from Maryland southward. In six hours the surface low deepened to 1008 mb and a surface cold front is analyzed. By 12 UTC 16 January, an upper-level cut-off low formed with a height of 558 decameters situated just west of the now rapidly deepening surface low. The storm subsequently deepened to 992 mb and moved zonally to 32°N 62°W by 00 UTC 17 January. The storm achieved a maximum deepening rate of 1.5.

The IWV field from the SSMI at 10 UTC 16 January, prior to deepening, is shown in figure 1. In the region east of the cold front, along the prefront trough (dashed line in figure) and south of the warm front, the moisture content is high. Maximum values of 44 kg m^{-2} are evident along the trough. The region where the water vapor content is greater than 30 kg m^{-2} is 85.0 x 10^4 km^2.

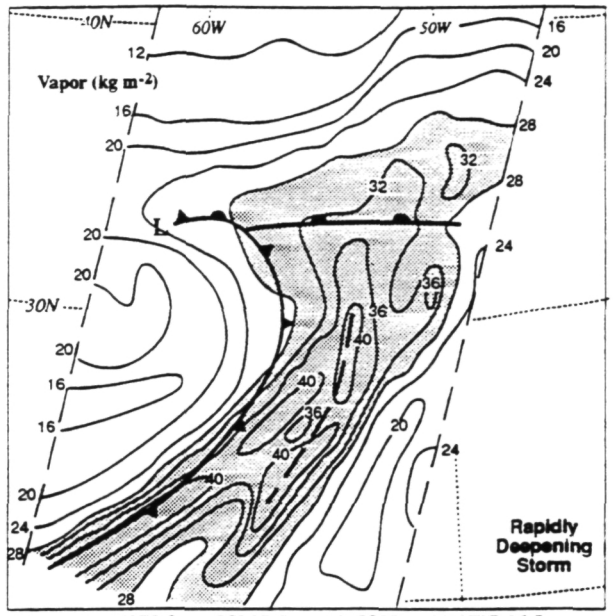

Figure 2 - IWV from SSM/I for orbit 2977 at 22 UTC 16 January 1988. The field is contoured every 4 kg m^{-2} and the region greater than 28 kg m^{-2} is shaded. Frontal analysis is estimated from the NMC hemispheric surface charts at 18 UTC 16 Jan. and 00 17 Jan.

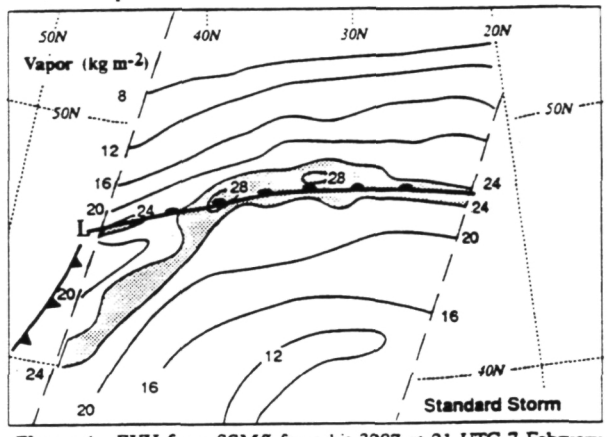

Figure 4 - IWV from SSM/I for orbit 3287 at 21 UTC 7 February 1988. The field is contoured every 4 kg m^{-2} and the region greater than 24 kg m^{-2} is shaded. Frontal analysis is estimated from the NMC hemispheric surface charts at 18 UTC 7 February and 00 UTC 8 February.

In figure 2, the IWV field at 22 UTC 16 January after rapid deepening is shown. The water vapor content is still high from the warm front southwards. Maximum water vapor content of 40 kg m^{-2} is evident at the trough and cold front, and the areal extent of water vapor content greater than 30 kg m^{-2} is still large, approximately 95.0 x 10^4 km^2. The water vapor pattern has evolved into a comma shape, and the strength of the water vapor gradient behind the cold front has increased.

3.2 Standard Cyclone: 6 - 8 February 1988

This storm developed from a wave on a pre-existing surface cold front. At 12 UTC, a closed low of 1012 mb is analyzed at 30°N 73°W at the cold front. The surface low did not begin to deepen until 12 UTC 7 February when a rapidly moving upper-level shortwave trough moved just upstream of the surface low. The surface low progressed northeastward to 46°N 54°W and deepened to 992 mb by 00 UTC 8 February. The storm had a maximum deepening rate of 1.0.

The IWV field at 23 UTC 6 February, prior to deepening, is shown in figure 3. In contrast to figure 1, high water vapor content is confined to a narrow band along the front and in a narrow region south of the front. The maximum water vapor content in this region is only 32 kg m^{-2}, and the region where the IWV content is greater than 30 kg m^{-2} is only 30.0 x 10^4 km^2.

In figure 4, the IWV pattern at 21 UTC 7 February is shown. At this stage, the low has moved substantially northward and the water vapor content is significantly lower than in figure 3. The maximum water vapor content is 28 kg m^{-2} along the warm front. The next orbit over this storm (Orbit 3288, not shown) samples the southern end of the cold front. Eventhough the front is south of 30°N, the maximum IWV content is also low, 36 kg m^{-2}, and confined to a narrow region along the front.

3.3 Summary of all cases

It was shown above that the rapidly deepening case exhibited substantially more water vapor content throughout its development than the standard case. In order to examine if this relationship holds for all cases, average maximum water vapor content and average area of IWV content greater than 30 kg m^{-2} were calculated for all the storms examined to date and are displayed in tables 2 and 3 respectively. In table 2, the average maximum IWV content is higher in rapidly deepening storms than in standard storms during both stages. However, since the number of samples is small and the standard deviations large, the averages are not significantly different at a confidence level of 90% or greater.

In table 3, average area of IWV content greater than 30 kg m^{-2} for storms is shown. Since the swath width of the SMMR is half that of the SSM/I, it is only possible to compare results from each instrument separately. In the SMMR standard cases, during the inicipient stage, only three of the eight storms had any IWV values greater than 30 kg m^{-2}, and of those three, the areal extent was quite small. In contrast, the areal extent of high vapor content for the SMMR rapidly deepening cases during their incipient stage was on average a factor of ten times larger. Therefore, despite the very large standard deviations and small number of cases, the average area of IWV content greater than 30 kg m^{-2} is significantly larger for SMMR rapidly deepening cases at the 95% confidence level. During the deepening stage, and for the SSM/I cases, the differences between rapidly deepening cyclones and standard cyclones are not significant due to large standard deviations and small number of cases.

Table 2 - Average maximum water vapor content for rapidly deepening and standard cyclones during the incipient and deepening stages. Ave denotes the average in kg m^{-2} , s.d. denotes the standard deviation and n the number of cases used.

A) RAPIDLY DEEPENING

	Incipient			Deepening		
	ave.	s.d.	n	ave.	s.d.	n
SMMR	27.6	7.3	6	32.5	6.5	12
SSM/I	36.7	7.0	3	36.2	4.7	4
together	30.4	8.1	9	34.2	6.1	16

B) STANDARD CYCLONES

	Incipient			Deepening		
	ave.	s.d.	n	ave.	s.d.	n
SMMR	26.4	5.5	9	31.3	5.0	13
SSM/I	34.3	2.3	2	35.0	1.4	2
together	27.9	5.9	11	31.7	4.8	15

Table 3 - Average area in warm sector where the IWV is greater than 30 kg m^{-2} for rapidly deepening and standard cylones. Ave denotes the average area in 10^4 km^2, s.d is the standard deviation and n is the number of samples used.

A) RAPIDLY DEEPENING

	Incipient			Deepening		
	ave.	s.d.	n	ave.	s.d.	n
SMMR	53.6	78.5	5	35.6	20.1	8
SSM/I	43.6	13.1	3	56.2	32.2	4

B) STANDARD CYCLONES

	Incipient			Deepening		
	ave.	s.d.	n	ave.	s.d.	n
SMMR	5.5	9.1	8	27.3	23.6	13
SSM/I	34.3	21.2	2	30.1	1.2	2

4. RAIN

The rain distribution given by the P_{37} fields from the SSM/I for the two storms discussed in the previous section are given in figures 5 and 6. The area covered by precipitation is quite extensive in the rapidly deepening case, figure 5. In addition, there are several areas of intense rainfall, evident as P_{37} values of 0.2 or less located along the trough, cold front and north and west of the developing surface low. In order for the latent heat of condensation (by precipitation) to influence the development of the surface low, the laplacian of the heating, not just the heating itself, is important (e.g., see eq. 3 in Kuo et al., 1991). Near the low center and cold front, non-raining areas are in close proximity to raining areas. Although it is not possible to calculate the magnitude of the latent heating, the spatial pattern of precipitation alone indicates that the contribution to the development of the low by diabatic heating may be important in this case.

In figure 6, the precipitation area is smaller than in the rapidly deepening case. In addition, the regions of intense rainfall are much fewer and smaller in this case. Furthermore, the raining areas are more continuous in the vicinity of the developing low center and the spatial pattern of rain is less complex. Again, it is not possible to calculate the magnitude of the latent heating; however, the rain distribution indicates that the contribution by diabatic heat to the low development may be less in this case than in the rapidly deepening case.

In table 4, the average area covered by precipitation in rapidly deepening and standard cyclones are presented. Due to the different swath widths and the different ways of indicating rain, the SMMR and SSM/I cases must be considered separately. During the incipient stage, the SMMR standard cases had very light rainfall, and three of the eight cases exhibited no rain. The average rain area for incipient rapidly deepening cyclones is significantly larger than the average rain area for incipient standard cyclones at the 95% confidence level. In addition, the average rain areas are significantly different during the deepening stages at the 90% confidence level. The differences between rapidly deepening and standard cyclones for the SSM/I cases are not significant due to the small number of cases.

5. SUMMARY

In this paper we present IWV and P_{37} analyses for thirty-four rapidly deepening and standard cyclones that occurred in the North Atlantic during the winters of 1979 - 1982 and 1988. We found that the maximum water vapor content was not significantly different in these two types of storms. Yet, during the incipient stage in the SMMR cases analyzed, the area of IWV amounts greater than 30 kg m^{-2} in the warm sector and the area of precipitation were significantly larger in rapidly deepening cyclones than in standard cyclones. The examples presented in section 4

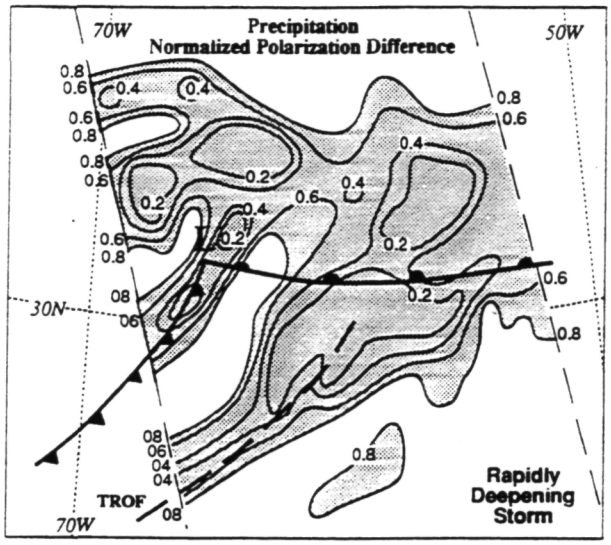

Figure 5 - P_{37} from SSM/I for orbit 2970 at 10 UTC 16 January 1988. The field is contoured every 0.2 and the region less than 0.8 indicates rain and is shaded. Frontal analysis is estimated from the NMC hemispheric surface charts at 06 and 12 UTC 16 January.

Table 4 - Average rain area where P37 is less than 0.8 for rapidly deepening and standard cylones. Ave denotes the average area in 10^4 km^2, s.d is the standard deviation and n is the number of samples used.

A) RAPIDLY DEEPENING

	Incipient			Deepening		
	ave.	s.d.	n	ave.	s.d.	n
SMMR	12.8	8.7	5	17.8	10.0	11
SSM/I	94.6	20.3	3	72.2	32.1	4

B) STANDARD CYCLONES

	Incipient			Deepening		
	ave.	s.d.	n	ave.	s.d.	n
SMMR	3.5	3.7	8	10.4	11.5	10
SSM/I	128.1	74.9	2	99.8	67.9	2

demonstrated that differences in rainfall intensity and rainfall pattern variability may exist between rapidly deepening and standard storms. However, more cases need to be analyzed in order to quantify these differences. The results obtained from the cases studied to date are consistent with the hypothesis that moisture availability and latent heating are important in the development of rapidly deepening cyclones.

Acknowledgments - We are grateful to Erika Francis and Frank Wentz of Remote Sensing Systems, Inc. who generously provided the SSM/I data tapes. The SMMR CELL-ALL data tapes were provided by the National Space Science Data Center at Goddard Space Flight Center. Special thanks are extended to Iftekar Bhatti for assistance in the SMMR analysis and Zhao Hongwei for assistance in the SSM/I analysis. We thank Ms. Kay Dewar for expertly drafting the figures. This work was supported by NASA Grants NAS8-36473 and NAGW-1688.

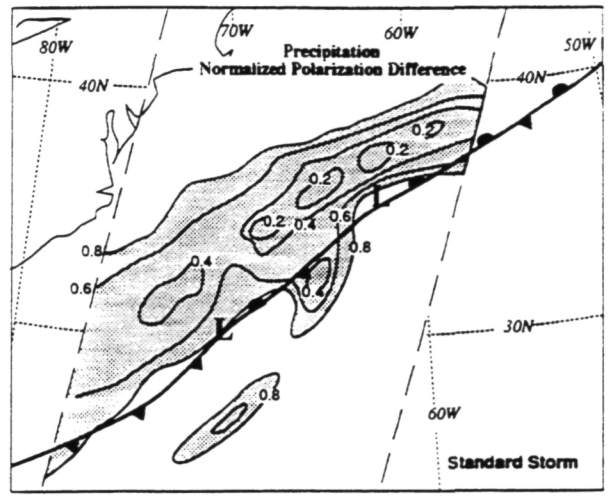

Figure 6 - P_{37} from SSM/I for orbit 3274 at 23 UTC 6 February 1988. The field is contoured every 0.2 and the region less than 0.8 indicates rain and is shaded. Frontal analysis is estimated from the NMC hemispheric surface charts at 00 UTC 7 February.

6. References

Chang, H.D., P.H. Hwang, T.T. Wilheit, A.T.C. Chang, D.H. Staelin and P.W. Rosenkranz, 1984: Monthly Distributions of Precipitable Water from the Nimbus 7 SMMR Data. *J. Geophys. Res.*, **89**, 5328-5334.

Katsaros, K.B., I. Bhatti, L. McMurdie and G. Petty, 1989: Identification of atmospheric fronts over the ocean with microwave measurements of water vapor and rain. *Weather and Forecasting*, **4**, 449-460.

Kuo, Y.-H., M. A. Shapiro and Evelyn G. Donall, 1991: The interaction between baroclinic and diabatic processes in a numerical simulation of a rapidly intensifying extratropical marine cyclone. *Mon. Wea. Rev.*,**119**, 368-383.

McMurdie, L.A. and K.B. Katsaros, 1985: Atmospheric water distribution in a mid-latitude cyclone observed by the Seasat Scanning Multichannel Microwave Radiometer. *Mon. Wea. Rev.*, **113**, 584-598.

McMurdie, L.A. and K.B. Katsaros, 1991: Satellite derived integrated water vapor distribution in oceanic midlatitude storms: variation with region and season. *Mon.Wea.Rev.*, **119**, 589-605.

Petty, G.W. and K.B. Katsaros, 1990: New geophysical algorithms for the Special Sensor Microwave/Imager. Preprint Volume, *Fifth International Conference on Satellite Meteorology and Oceanography*, September 3-7, 1990, London, England.

Rabin, R. M., L. A. McMurdie, C. M. Hayden and G. S. Wade, 1991: Monitoring precipitable water and surface wind over the Gulf of Mexico from microwave and VAS satellite imagery. *Wea. and Forecasting*, **6**, 227-243.

Reed, R.J., A.J. Simmons, M.D. Albright and P. Unden, 1988: The role of latent heat release in explosive cyclogenesis: three examples based on ECMWF operational forecasts. *Wea. & Forecasting*, **3**, 217-229.

Sanders, F., 1987: Skill of NMC operational dynamical models in prediction of explosive cyclogenesis. *Wea. and Forecasting*, **2**, 322-336.

Sanders, F. and J. R. Gyakum, 1980: Synoptic-dynamic climatology of the "Bomb". *Mon. Wea. Rev.*, **108**, 1589-1606.